Chemical Engineering Journal 161 (2010) 83–92

Contents lists available at ScienceDirect

Chemical Engineering Journal

journal homepage: www.elsevier.com/locate/cej

Photocatalytic degradation of lindane under UV and visible light using N-doped TiO_2

J. Senthilnathan, Ligy Philip*

Indian Institute of Technology Madras, EWRE Division, Department of Civil Engineering, Chennai 600036, Tamil Nadu, India

ARTICLE INFO

Article history:
Received 9 January 2010
Received in revised form 1 April 2010
Accepted 18 April 2010

Keywords:
N-doped TiO_2
Lindane
Triethylamine
Photocatalyst
Pesticide

ABSTRACT

Nitrogen doped titanium photocatalysts with different nitrogen containing organic compounds were prepared by sol–gel method in acidic media. Among different nitrogen containing organic compounds, triethylamine doped TiO_2 showed better photocatalytic activity under visible light. XRD, SEM and TEM analyses showed that the crystalline size of N-doped TiO_2 was in the range of 20–24 nm. XRD and Raman spectrum showed that all peaks of N-doped TiO_2 correspond to anatase crystalline structure. The formation of O–Ti–N bond in N-doped TiO_2 does not lead to any new Raman band. XPS study confirmed that N replaces the O in the lattice of TiO_2 and is present in the form of O–Ti–N. The photocatalytic activity of doped TiO_2 was measured under UV and visible light using lindane as a target pollutant. The photocatalytic activity of anatase TiO_2 and N-doped TiO_2 was compared with commercially available Degussa P-25 TiO_2. Intermediates formed during the degradation of lindane were monitored by GC–MS analysis.

1. Introduction

Increased awareness about the potential pesticides movement into the drinking water sources has compelled the researchers and policy makers to identify ways to prevent such contamination. Several studies reported the presence of organochlorine pesticide such as lindane residues in river, soil and groundwater in India [1,2]. Though the production of lindane in India has reduced as compared to its earlier production, India is still one of the highest lindane contaminated country in the world [3,4]. Most of the Indian rivers are passing through agricultural fields and they are subjected to contamination with different pesticides used for crop protection [5]. Hence, leaching of pesticide from agricultural fields is the single non-point source of pollution to the aquatic environment. Since rivers are the major source of water in India, water quality needs to be maintained. Though many conventional methods are available for the treatment of pesticides contaminated surface and groundwater sources, advanced oxidation method is the most effective technology for surface and groundwater treatment [6]. Titanium dioxide (TiO_2) remains the most promising photocatalyst because of its high efficiency, low cost, chemical inertness and photostability [7].

Several researchers have tried the degradation of lindane from drinking water sources using TiO_2 under UV light [8–10]. Zaleska et al. [10] have reported that anatase supported on glass hollow microspheres was able to degrade 50% of lindane (40 ppm initial concentration) within 150 min of processing time. Dionysiou et al. [9] have reported the degradation of lindane using TiO_2 immobilized on a continuous flow rotating disc and have achieved 63% of lindane (initial concentration 0.016 mmol/L) degradation. Senthilnathan and Philip [8] have reported the degradation of lindane using immobilized TiO_2 in single and mixed pesticides systems. In both cases complete degradation was achieved, however the rate of degradation of lindnae in single pesticide system (1 mg/L degraded within 230 min) was different from that in mixed (lindane, methyl parathion and dichlorvos) pesticides system (1 mg/L lindane degraded within 260 min). Though photocatalytic degradation of pesticide using TiO_2 under UV light is possible, it may not be a practical proposition for the treatment of drinking water sources due to the high cost. Efficient utilization of visible and solar light is one of the major goals of modern science and engineering that will have a great impact on technological applications [11]. Although advanced oxidation process with TiO_2 photocatalysts have been shown to be an effective alternative in this regard, the vital snag of TiO_2 semiconductor is that it absorbs a small portion of solar spectrum in the UV region (band gap energy of TiO_2 is 3.2 eV). To utilize maximum solar energy, it is necessary to shift the absorption threshold towards visible region [12,13].

The shifting of TiO_2 absorption into visible light region mainly focuses on the doping with transition metals [14]. However, the thermal instability, tendency to form charge carrier recombination centers, as well as the expensive ion implantation facilities make metal doped TiO_2 impractical [13,15]. TiO_2 absorption towards the visible light with non-metallic elements such as the nitrogen (N), sulphur (S), carbon (C) and phosphorus (P) have been reported in many literatures [16–22]. Insertion of N or S atoms in TiO_2

* Corresponding author. Tel.: +91 44 22574252; fax: +91 44 22574274.
E-mail address: ligy@iitm.ac.in (L. Philip).

1385-8947/$ – see front matter © 2010 Elsevier B.V. All rights reserved.
doi:10.1016/j.cej.2010.04.034

produces localized states within the band gap just above the valence band. Thus, when N or S doped TiO_2 is exposed to visible light, electrons are promoted from these localized states to the conduction band [16,17]. The substitutional (N–Ti–O) doping of N was most effective compared to other non-metal dopants (S, P and C) because its p states contribute to the band-gap narrowing by mixing with O 2p states [13,24]. Even though doping with S shows a similar band-gap narrowing, it requires larger formation energy for the substitution than that required for the substitution of N. Moreover, the ionic radius of S is larger than O thus difficult to fit in into the TiO_2 crystal [13].

Xing et al. [24] have reported that N-doped TiO_2 synthesized using ammonium nitrate and ammonia as a nitrogen sources showed maximum photocatalytic activity for the degradation of 2,4-dichlorophenol (initial concentration 100 mg/L) within 5 h of irradiation under visible light. Ananpattarachai et al. [23] have reported that the degradation of 2-chlorophenol (initial concentration 25 mg/L) using N-doped TiO_2 under visible light followed pseudo first order reaction and complete degradation was achieved within 50 min of irradiation [23]. Similar study was conducted by Cong et al. [25], with 2-4-dichlorophenol (100 mg/L) and rhodamine B (20 mg/L) using N-doped TiO_2 under visible light and complete degradation was obtained within 5 h and 1 h of irradiation, respectively. Huan et al. [26] have studied the decomposition of 4-chlorophenol (13 mg/L) using N-doped TiO_2 under visible light and achieved 63.5% degradation within 6 h of irradiation time. Kun et al. [27] have studied the photocatalytic activity of phenol (0.5 mmol/L) under visible light with N-doped TiO_2 and found that acid treated N TiO_2 showed higher catalytic activity within 2 h of irradiation. Many researchers have worked on simple organic compounds like methylene blue [28,29], toluene [30], benzamide [31], phenol [32] and methyl violet [33]. However, so far no attempt was made to degrade lindane or any other organochlorine pesticides using N-doped TiO_2 under visible light.

The present study is focused on the preparation of N-doped TiO_2 using different nitrogen containing organic compounds. Their photocatalytic activity was measured using lindane as a target pollutant under UV and visible light. Characterization of N-doped TiO_2 was carried out using XRD, XPS, TGA, TEM, SEM, UV–vis, Raman and FTIR spectrometer techniques. The lindane degradation was carried out with anatase TiO_2, N-doped TiO_2 and commercially available Degussa P-25 TiO_2 and their kinetics was measured under UV as well as visible light.

2. Materials and methods

2.1. Chemicals used

Titanium isopropoxide (purity over 98%), isopropanol, triethylamine, urea, ethylamine, silver nitrate, ferric chloride, chromium chloride and ethyl alcohol purchased from Ranbaxy Chemicals, India, were used for the preparation of metal ion doped TiO_2 and N-doped TiO_2. Lindane (HPLC grade) used in the present study was procured from Ranbaxy Chemicals, India. Titanium dioxide (Degussa P-25), which is a known mixture of 70% anatase and 30% rutile with an average crystalline size of 30 nm and a non-porous material with a reactive surface area of 50 m^2/g, was supplied by Vicas Rane, India Limited, Bombay, India.

2.2. Preparation of metal and non-metal ion doped TiO_2

2.2.1. Preparation of metal ion doped TiO_2

The preparation of chromium (Cr) doped TiO_2 and Cr–N co-doped TiO_2 was carried out by sol–gel process. Precursor chromium chloride was dissolved in ethanol and then mixed with titanium isopropoxide. The volume of ethanol was 10 times higher than that of titanium isopropoxide and the amount of chromium chloride was calculated based on the desired Cr/Ti percentage (0.5%, 1.0%, 1.5%, 2.0% and 2.5%). For Cr–N co-doped TiO_2, fixed amount of triethylamine (1 mL) was added to all the five different concentration chromium and titanium isopropoxide solution. The mixed solution was slowly added to equal volume of 0.1 M HCl solution and quickly stirred until a clear solution was obtained. The solution was autoclaved at 80 °C for 12 h. The suspension was centrifuged at 8000 rpm and residue was dried at 100 °C for overnight. The dried gel was then calcined in air atmosphere at 550 °C for 4 h. Ag and Fe doped TiO_2 also was prepared by above process. 1000 mg/L of Ag and Fe solutions were prepared using $AgNO_3$ and anhydrous $FeCl_3$ salt. The required concentration (0.5%, 1.0%, 1.5%, 2.0% and 2.5%) of Ag doped TiO_2 and Fe doped TiO_2 was prepared by mixing various concentrations of above prepared solutions with ethanol and titanium isopropoxide solution. The rest of the procedure was similar to that of Cr doped TiO_2 preparation.

2.2.2. Preparation of non-metal (nitrogen) ion doped TiO_2

Preparation of N-doped TiO_2 was carried out by the hydrolysis of titanium isopropoxide. 2.4 mL of titanium isopropoxide was dissolved in 20 mL ethyl alcohol and suitable ratio (1:0.4, 1:0.8, 1:1.2, 1:1.6 and 1:2.0 ratio of N:Ti) of nitrogen containing organic compound (triethylamine) was added to it. 20 mL of 0.1 M of HCl was added to the above solution and stirred to get a clear liquid. The above solution was autoclaved at 80 °C for 12 h. The suspension was centrifuged at 8000 rpm and residue was dried at 100 °C. The dried sample was calcined at 550 °C for 4 h. Similar procedure was followed for the preparation of anatase TiO_2 without the addition of nitrogen and N-doped TiO_2 using other nitrogen containing organic compound like urea, ethyl amine and ammonium hydroxide.

2.3. Analytical methods

The concentration of lindane was analyzed using PerkinElmer Clarus 500 gas chromatograph (GC) with electron capture detector (GC/ECD) equipped with auto-sampler, an on-column, split/split less capillary injection system and with PerkinElmer (PE)-5 capillary column (30 m × 0.53 mm × 0.5 μm film thickness). The operating conditions were as follows: the column was initially held at a temperature of 100 °C for 1 min and then the temperature was increased at a rate of 10 °C/min to 260 °C and finally held at 260 °C for 1 min. The temperatures of injector and detector were maintained at 200 and 350 °C, respectively. The intermediates formed during the degradation of lindane were monitored using a GC–MS, supplied by Agilent, USA, and a temperature program similar to the one used for GC analysis was employed for the GC–MS analyses also. The crystalline structure modification of N-doped TiO_2 was examined by X-ray diffraction (XRD) analyses using Copper K alpha radiation with Lynx detector at an operating voltage of 35 kV and current of 25mamps supplied by Bruker Axs, USA (model D8 Discover). Varian Cary-5E UV–vis-NIR, scan range 185–3000 nm (UV–vis-NIR) high-resolution spectrophotometer was used to find the UV and visible light absorption pattern of anatase and N-doped TiO_2. FTIR spectrometer supplied by PerkinElmer Spectrum one, scan range of MIR 450–4000 cm^{-1} and resolution 1.0 cm^{-1} was used. The surface morphology and crystalline size of N-doped TiO_2 were monitored using a scanning electron microscope (SEM) equipped with a field emission gun (JEOL, JSM-6380, Japan) and high-resolution transmission electron microscopy (HRTEM) using JEOL 3010 UHR instrument. The SL films were lifted on carbon coated copper grid sand dried in ambience. The sample was observed at 200 keV to reduce electron beam induced damage. X-ray photoelectron spectroscopy (XPS) measurements were carried out using an Omicron Nanotechnology spectrometer with poly-

chromatic Al Kα X-rays (hν = 1486.6 eV). At least ten spectra in the desired binding energy range were collected and an average was taken. The samples were spotted as drop cast films on the sample stub and dried under vacuum. X-ray flux was adjusted to reduce the beam induced damage of the sample. The energy resolution of the spectrometer was set at 1.1 eV at pass energy of 50 eV. Binding energy (BE) was calibrated with respect to C 1s (285.0 eV). The Raman spectrum and corresponding imaging were done using a Witec Gmb Hconfocal Raman spectrometer equipped with 514.5 and 532 nm sources with a spot size <1 μm. The laser had a maximum power of 40 mW. The excitation laser was focused using a 100 objective and the signal was collected in a back scattering geometry and guided to a Peltier-cooled charge-coupled device (CCD) detector and the signal was dispersed using an 1800 grooves/mm grating. Concentration of free chloride ions was analyzed using ion chromatography (IC) supplied by Dionex, USA, with Electro Chemical Detector (ED50).

2.4. Experimental methodology

2.4.1. Immobilization of doped TiO_2

A Pyrex glass tube with an inner surface area of 169.56 cm^2 (with a height of 90 mm and a diameter of 60 mm) was coated by the photocatalyst. Before coating, the inner surface of the Pyrex glass tube was treated with 5% (v/v) hydrofluoric acid for 30 min to get a rough surface and then washed with distilled water. The Pyrex glass tube coating was carried out using 0.5% suspension of N-doped TiO_2 in isopropanol. Before coating, the suspension was sonicated for 15 min and the Pyrex tube was inserted slowly into the suspension. It was allowed to stay for 5 min, then taken out and dried in an oven for 30 min at 150 °C. The weight of coated TiO_2 was monitored each time.

2.4.2. Photo reactor

Photocatalytic degradation of lindane was performed in an immobilized batch reactor. A cylindrical photochemical reactor with a volume of 400 mL was provided with water circulation arrangement to maintain the temperature in the range of 25–30 °C. Irradiation was carried out with 500 W high pressure tungsten visible lamp, supplied by Haber Scientific, India, which emitted radiation at a wavelength of >400 nm. For immobilized batch reactor, coated Pyrex tube was inserted into the reactor. Before adding lindane, the visible lamp was warmed up for 15 min to attain sufficient energy. Oxygen flow rate of 300 mL/min and a stirring rate of 150 rpm were maintained in all the experiments. Samples were collected at regular intervals and extracted with HPLC grade n-hexane (purity 99%) and analyzed using GC. The stock solutions of lindane for desired concentration were prepared in double distilled water and HPLC grade acetone. A schematic diagram of the photoreactor employed in the present study is given in Fig. 1.

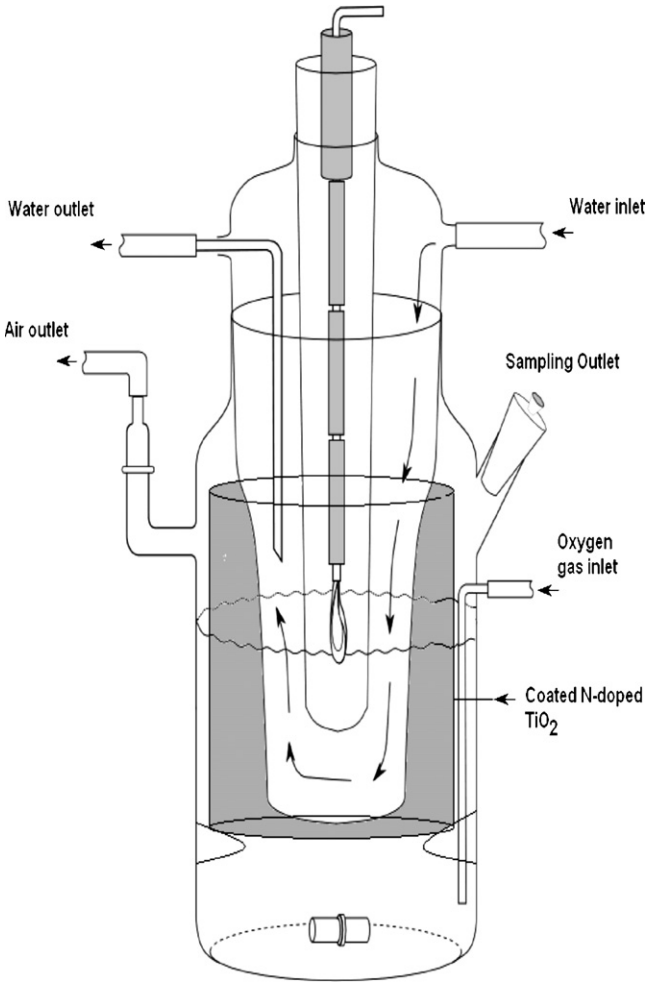

Fig. 1. Schematic diagram of photo reactor.

3. Results and discussion

3.1. Photocatalytic properties of different ions doped TiO_2

TiO_2 is not an efficient catalyst under visible light. In order to explore the possibilities of using photoctalytic degradation of pesticides under visible light, different metal/non-metal doped TiO_2 were prepared (Ag^+, Fe^{3+}, Cr^{3+} doped TiO_2 and Cr^{3+}–N co-doped $TiO_{2-x}N_x$) by sol–gel process. Photocatalytic activity of Ag^+, Fe^{3+}, Cr^{3+} doped TiO_2 and Cr^{3+}–N co-doped TiO_2 were assessed using lindane (3.44×10^{-4} mmol/L) as a target pollutant. A fixed reaction time of 7 h and 3.44×10^{-4} mmol/L concentration of lindane were maintained for preliminary screening of metal doped TiO_2. The doping concentration was varied from 0% to 2.5% for all the metal ions. The degradation of lindane under visible light using different metal doped TiO_2 is given in Fig. 2. Maximum degradation of 10.2% and 23.45% of lindane were achieved for Fe^{3+} and Ag^+ doped TiO_2, respectively. Cr^{3+}–N co-doped TiO_2 showed maximum degradation of 43.42%, whereas Cr^{3+} doped TiO_2 showed only 30.3% lindane degradation. As evident, Cr^{3+}–N co-doped TiO_2 showed better photocatalytic activity compared to Cr^{3+}, Fe^{3+} and

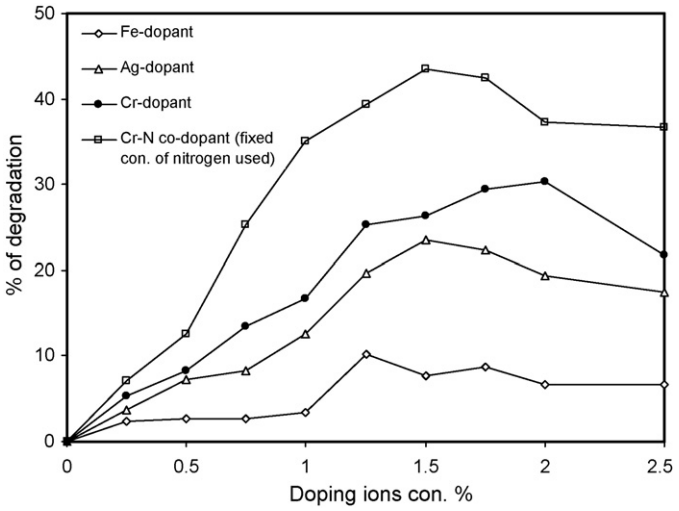

Fig. 2. Lindane degradation by Ag, Fe, Cr and Cr–N co-doped TiO_2.

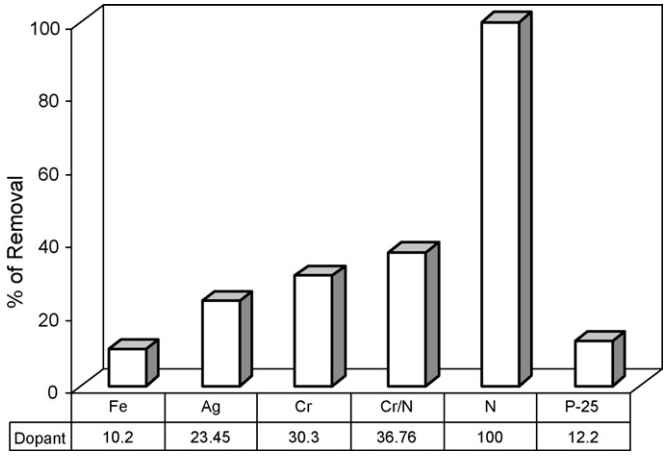

Fig. 3. Comparison of lindane degradation efficiency of N-doped TiO_2 with metal ions doped TiO_2.

Ag^+ doped TiO_2 under visible light. None of the metal doped TiO_2 catalyst showed complete degradation of lindane within the stipulated reaction time of 7 h. Hence, anion doping (nitrogen doping) was tried with titanium isopropoxide and triethylamine in the ratio of 1:1.6 under similar condition. Performance of N-doped TiO_2, Ag^+ doped TiO_2, Fe^{3+} doped TiO_2, Cr^{3+} doped TiO_2 and Cr^{3+}–N co-doped TiO_2 are given in Fig. 3. N-doped TiO_2 showed better photocatalytic activity compared to other metal ions doped TiO_2. Complete degradation of lindane (3.44×10^{-4} mmol/L) was achieved in presence of N-doped TiO_2 within 5.5 h of irradiation. Hence, N-doped TiO_2 was used for further studies.

3.2. Effect of different nitrogen containing organic compounds

The N-doped TiO_2 was prepared using triethylamine, urea, ethylamine and ammonium hydroxide by sol–gel process. Photocatalytic activity of N-doped TiO_2 was compared with Degussa P-25 TiO_2 and photodegradation studies were carried out with 3.44×10^{-4} mmol/L of lindane. The N-doped TiO_2 prepared by different nitrogen containing compounds was compared with each other and the results are given in Fig. 4. Photocatalytic activity was much higher for triethylamine doped TiO_2 as compared to urea, ethyl amine and ammonium hydroxide doped TiO_2 [23,25]. Triethylamine doped TiO_2 showed greater photocatalytic activity.

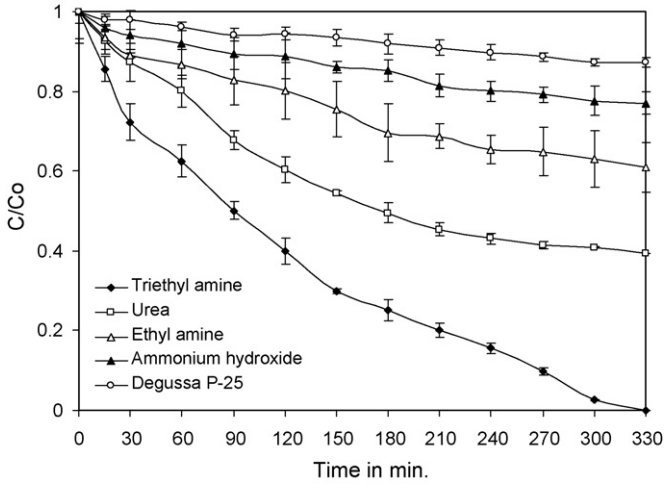

Fig. 4. Kinetics of lindane degradation by N-doped TiO_2 prepared using various nitrogen containing organic compounds.

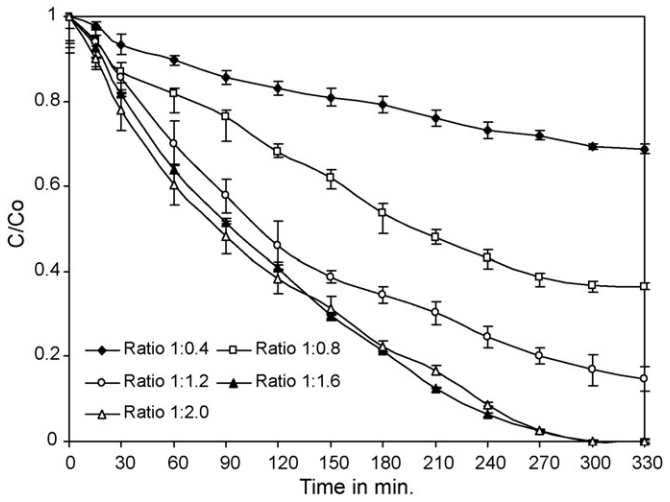

Fig. 5. Effect of nitrogen concentration in (triethylamine) N-doped TiO_2 on lindane degradation.

Triethylamine is a tridentate ligand, which forms a stable organo titanium complex compared to urea, ammonium hydroxide and ethylamine. This complex plays a very important role on the stability of the nano-particles and avoids the growth and aggregation of the particles [33]. This may be the reason for the higher photocatalytic activity of triethylamine doped TiO_2. Hence, triethylamine doped TiO_2 was used for rest of the studies. Only 5% degradation occurred with Degussa P-25 TiO_2 was used under visible light.

3.3. Effect of triethylamine concentration on doped TiO_2

The photocatalytic activity of different grades of N-doped TiO_2 prepared by varying the molar ratio of titanium isopropoxide and triethylamine was monitored. The molar ratios of Ti:N used in the present study were 1:0.4, 1:0.8, 1:1.2, 1:1.6 and 1:2.0. Fixed concentration of lindane (3.44×10^{-4} mmol/L) was used for all degradation studies and the results are given in Fig. 5. The rate of degradation was increased with increasing triethylamine concentration up to 1:1.6 ratio and complete degradation was achieved within 330 min of irradiation. Beyond this ratio there was no change in the rate of degradation of lindane. Xing et al. [24] and Cong et al. [25] have reported that photocatalytic activity of N-doped TiO_2 increased with increase in the molar ratio of Ti:N up to 1:2, beyond this molar ratio the catalytic activity decreased rapidly. The photocatalytic activity of N-doped TiO_2 improves by the increasing Ti:N ratio in the catalyst. However, the photocatalytic activity decreases due to chemically adsorbed nitrogen on TiO_2 lattice. The increase in nitrogen ratio causes chemical adsorption and the chemically adsorbed nitrogen covers the surface of the catalyst and decreases the number of active sites [24,34]. The optimum molar ratio of Ti:N (1:1.6) was used for the rest of the studies.

3.4. Characterization of N-doped TiO_2

The effect of nitrogen concentration was investigated for TiO_2 modified with triethylamine and its characterization was done. Physical characterization of N-doped TiO_2 was carried out using UV–visible spectrometer, X-ray diffraction (XRD), X-ray photoelectron spectrometer (XPS), Raman spectrometer, Fourier transformed infrared spectroscopy (FTIR), transmission electron microscope (TEM), thermo gravimetric analysis (TGA) and scanning electron microscope (SEM) analysis.

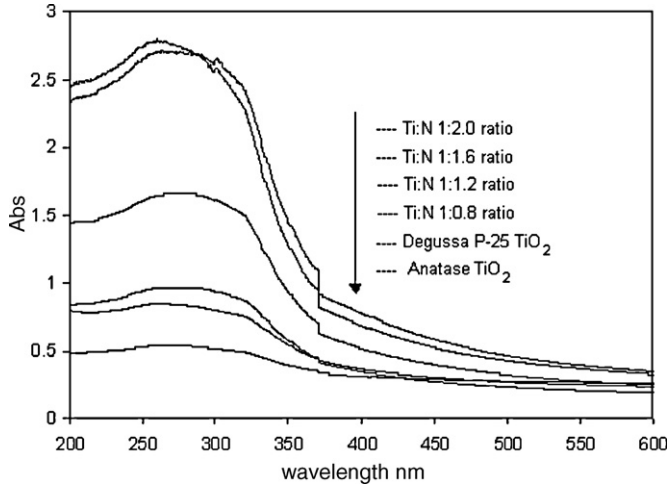

Fig. 6. UV–visible absorption of Degussa P-25, anatase TiO_2 and N-doped TiO_2.

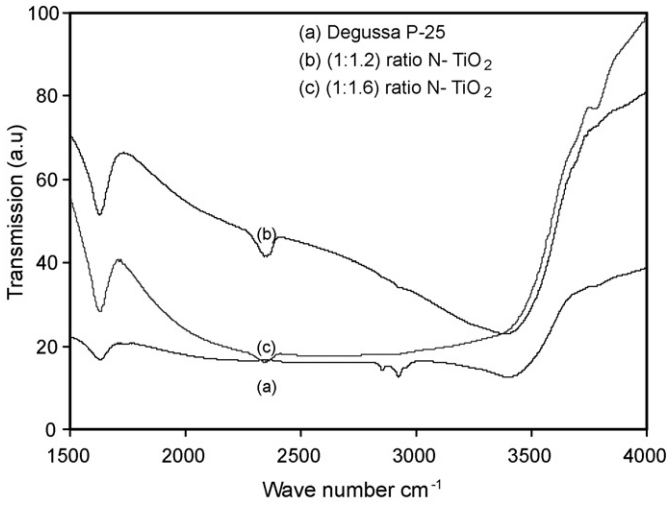

Fig. 7. FTIR spectrum of Degussa P-25 and N-doped TiO_2.

3.4.1. Optical properties of N-doped TiO_2

UV–visible spectroscopy is the most commonly used technique to study the optical properties of N-doped TiO_2. Most of the studies showed that the N-doped TiO_2 exhibited increased absorption between 400 and 600 nm, which depended on the experimental conditions and nature of nitrogen containing organic compound used for the doping study [35]. The UV–vis absorption spectrum for N-doped TiO_2 (1:0.8, 1:1.2, 1:1.6 and 1:2.0 ratio), anatase TiO_2 and Degussa P-25 TiO_2 were studied and the results are presented in Fig. 6. The optical absorption edges of the N-doped TiO_2 shifted to the lower energy region compared to those of the Degussa P-25 and anatase TiO_2 and the absorption of light in the wavelengths ranging from 400 to 600 nm was stronger after nitrogen doping. Furthermore, the absorption increases with increasing doping concentration from 1:0.8 to 1:2.0 and the results showed that band gap energies of all N-doped TiO_2 were lower than those of anatase TiO_2 and Degussa P-25. The reduction in the band gap energy of the N-doped TiO_2 sample was determined by the following equation [36].

$$E_g = \frac{1239.8}{\lambda} \quad (1)$$

where E_g is the band gap (eV) and λ is the wavelength (nm) of the absorption edge in the spectrum. The band gap was shifted from 3.20 to 2.91 eV for (1:1.6 ratio) N-doped TiO_2. This decrease in bandwidth will enhance the transfer of electron from valance band to conduction band under visible light. This may be the reason for the better performance of N-doped TiO_2 compared to other metal ions doped TiO_2.

3.4.2. FTIR spectroscopy of N-doped TiO_2

An FTIR spectrum gives an idea about surface functional groups of N-doped TiO_2. The FTIR spectra of different photocatalysts are shown in Fig. 7. The main absorption peaks were located at 3410, 2845, 2916, 2340 and 1623 cm^{-1} in all the three samples. The broad adsorption band observed at 2900–3600 cm^{-1} corresponds to the O–H stretch region [37]. The peaks at 3450–3420 and 1640–1630 cm^{-1} were assigned to the O–H stretching vibration and the adsorbed H_2O bending vibration. The absorption peak at 2345 cm^{-1} is characteristic of surface adsorbed CO_2 [38]. The typical infrared peaks of NO_2 occur at 1618 cm^{-1} (antisymmetric stretch, very strong). Triethylamine displays sharp peaks at 2950 cm^{-1}. Such a peak was not obtained for N-doped TiO_2. Thus, it can be inferred that there was no organic residue in any of the N-doped TiO_2 photocatalysts.

3.4.3. Thermo gravimetric analysis (TGA) profile of N-doped TiO_2

The thermo gravimetric profile of N (triethylamine) doped TiO_2 (before calcinations to 550 °C) was carried out. In the present study a temperature range of 25–1000 °C was used and at the end of the analysis around 75% weight loss was observed. The decomposition temperature of N-doped TiO_2 showed two regions 60–230 and 230–525 °C. The thermal decomposition profile (TG) of N-doped TiO_2 is shown in Fig. 8. It was believed that the weight loss in the first region was due to the adsorbed water and the second region was due to the decomposition of excess triethylamine. Beyond 550 °C slight weight losses has been observed this could be ascribed to the decomposition of residuals. Similar trend in thermal decomposition profile was reported by Sathish et al. [29].

3.4.4. XRD analysis for different ratio of N-doped TiO_2

X-ray diffraction (XRD) is a very important technique employed for the characterization of doped TiO_2. From the intensity of the particular reflections, the X-ray diffraction patterns and average crystalline size can be calculated [39]. X-ray diffraction patterns for different grades of N-doped TiO_2 are presented in Fig. 9. All the N-doped TiO_2 samples showed X-ray line broadening compared to TiO_2, representing the formation of nano-particles. The broadening of the peak gradually increased up to 1:2.0 ratio of

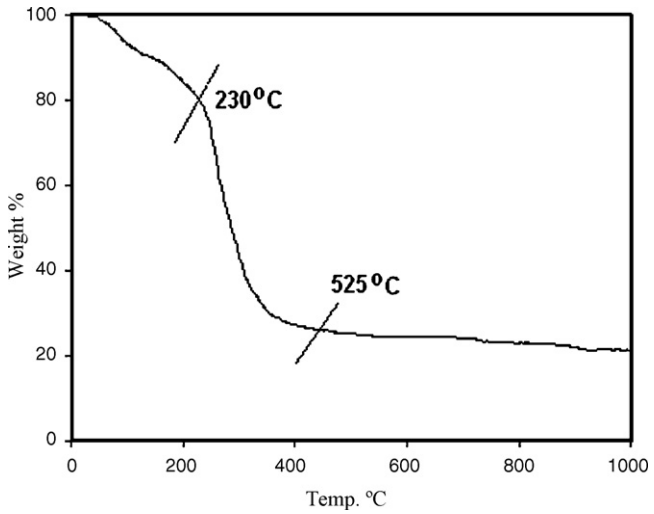

Fig. 8. TGA profile of (1:1.6 ratio) N–TiO_2.

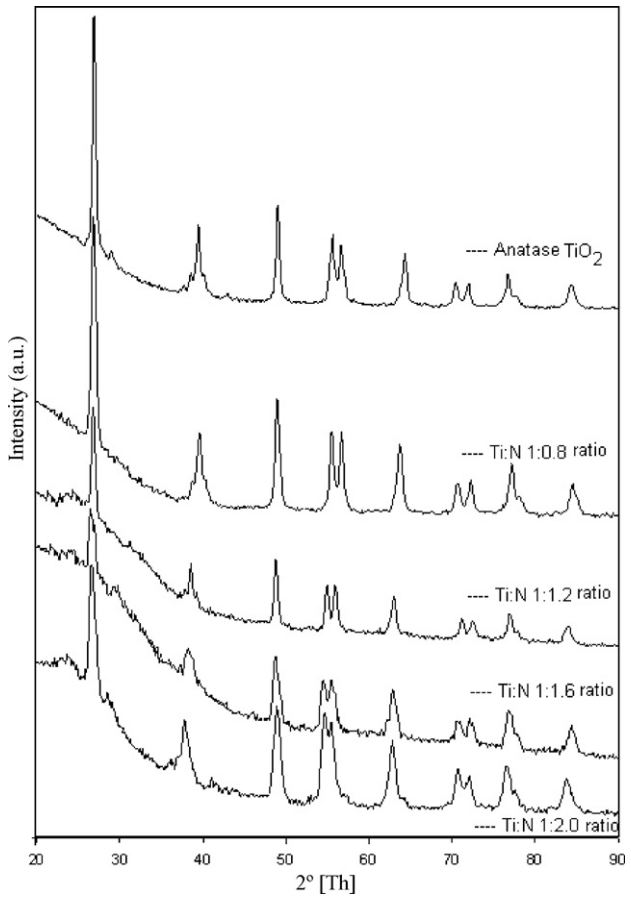

Fig. 9. XRD for different grades of N-doped TiO_2 and anatase TiO_2.

N-doped TiO_2. However, no significant changes were observed by further increasing the N ratio. The broadening of the XRD peaks is inversely proportional to the crystalline size of the N-doped TiO_2 nano-particles [25]. This indicates that N doping was introduced into the lattice of the TiO_2 without altering the average unit cell dimension and the similar trend was reported by Khan et al. [40]. Determination of crystal size of anatase TiO_2 and N-doped TiO_2 was done using Scherrer equation.

$$D = \frac{K\lambda}{\beta \cos\theta} \quad (2)$$

where D is the size of the crystal grain, K is a dimensionless constant (0.9), 2θ is the diffraction angle, λ is the wavelength of the X-ray radiation and β is the full width at half-maximum (FWHM) of the diffraction peak. The values of β and θ are taken for crystal plane (1 0 1) of anatase phase. The crystal grain size of TiO_2 bulk and N-doped TiO_2 calculated by Scherrer equation are given in Table 1. The crystal grain size of bulk TiO_2 was 70.3 nm and by increasing the amount of N-doped in to the TiO_2, the crystallite size gradually decreased and reached minimum value of around 25.4 nm. Similar results are reported by Cong et al. [25]. The crystalline size of N-doped TiO_2 was further confirmed by SEM and TEM analysis. The crystalline size and morphology of TiO_2 catalyst were studied using Scanning Electron Microscope. It is clear from Fig. 10, that the size of TiO_2 particles is approximately 20–30 nm. The exact size of nano-particles is very difficult to determine using SEM analysis. Therefore TEM analysis was carried out to find the size of TiO_2. From the TEM analysis, it was found that the crystalline size of N-doped TiO_2 is ~22 nm. TEM analysis result of N-doped TiO_2 is given in Fig. 11.

Table 1
Determination of crystal grain size using Scherrer equation.

S. No	Photocatalyst	β (fwhm)	$\cos\theta$	Particle size (nm)
1	Anatase TiO_2	0.011808	0.0163	70.3
2	TiO_2/N (1:0.8)	0.014366	0.0167	56.2
3	TiO_2/N (1:1.2)	0.015044	0.0161	55.7
4	TiO_2/N (1:1.6)	0.031350	0.0169	25.4
5	TiO_2/N (1:2.0)	0.027281	0.0168	29.4

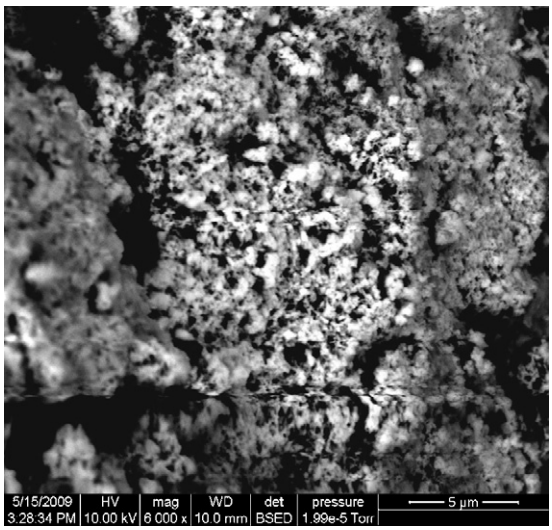

Fig. 10. SEM analysis of N-doped TiO_2 (1:1.6 ratio).

3.4.5. Raman spectrum of N-doped TiO_2

The Raman spectrum of TiO_2 peaks visible over the 400–700 cm^{-1} range are characteristic of anatase and rutile crystalline structures [41,42]. TiO_2 of anatase crystalline structure shows six Raman active fundamental modes correspondingly at 144 cm^{-1} (E_g), 197 cm^{-1} (E_g), 397 cm^{-1} (B_{1g}), 518 cm^{-1} ($A_{1g}+B_{1g}$) and 640 cm^{-1} (E_g) for crystalline anatase TiO_2. For rutile TiO_2, there are four Raman active modes at 144 cm^{-1} (B_{1g}), 448 cm^{-1} (E_g), 613 cm^{-1} (A_{1g}) and 827 cm^{-1} (B_{2g}), respectively [41,43]. The anatase TiO_2 and N-doped TiO_2 displayed Raman vibrations at around 146, 199, 400, 519 and 636 cm^{-1}. All peaks correspond to anatase crystalline structure and no rutile peaks was observed. Small peak shift was observed while comparing anatase TiO_2 and N-doped TiO_2. This is because of different crystalline sizes of

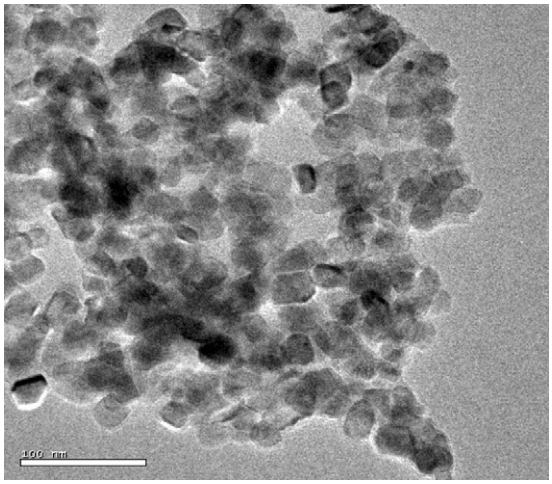

Fig. 11. TEM analysis of N-doped TiO_2 (Ti:N 1:1.6 ratio).

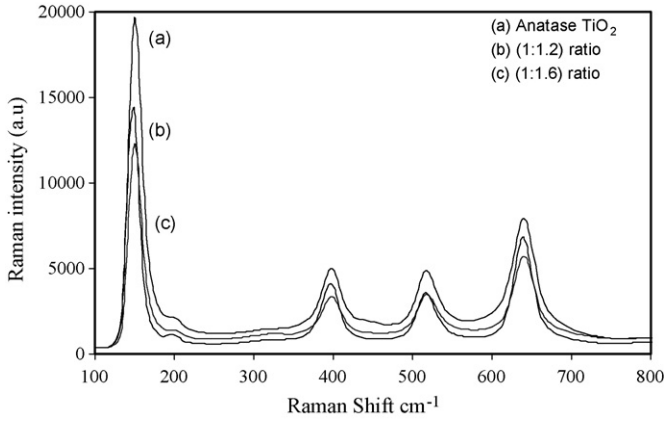

Fig. 12. Raman spectrums of anatase and N-doped TiO_2.

the anatase and N-doped TiO_2. The formation of O–Ti–N bond in N-doped TiO_2 does not lead to any new Raman band [44,45]. This could be a small change in the Raman vibrational modes due to the partial replacement of O with N and which is too small to be detected. The Raman spectrum of anatase TiO_2 and two different ratio of N-doped TiO_2 are given in Fig. 12.

3.4.6. X-ray photoelectron spectroscopy (XPS)

XPS analysis provides information about the chemical composition and electronic structures of element present on a surface and in depth. The XPS technique monitors the electron binding energy of elements within a few nanometers of the particle surfaces. The investigation of XPS for anatase TiO_2 and N-doped TiO_2 samples were examined for three areas of the XPS spectrum, the Ti 2p region near 460 eV, the O 1s region near 530 eV and the N 1s region near 400 eV. Most of the N 1s binding energies are found in between 396 and 408 eV [46,47]. However, the binding energy of the N 1s is highly dependent on the synthetic method used for the preparation of N TiO_2 and N 1s binding energies found around 396–397 eV were attributed to substitutional N in Ti–N, while peaks at higher binding energies (400 eV found in our case) were observed and usually ascribed to a generic interstitial site (O–Ti–N) [48]. This clearly indicates that the N-doped TiO_2 prepared by sol–gel process in the present study did not have N–Ti–N form where as O–Ti–N form was present in the catalyst.

XPS analysis of anatase TiO_2 and N-doped TiO_2 (1:0.8 and 1:1.6 ratio) are given in Fig. 13. Both ratio of N-doped TiO_2 showed peak at 400 eV after carbon correction. The peak at 400 eV indicates N atoms incorporated in to the TiO_2 lattice and it was observed that a peak towards 400 eV could be assigned to Ti bound to O or to the O–Ti–N formation [21]. From the above observations it can be concluded that the chemical states of the nitrogen doped into TiO_2 may be various and coexist in the form of N–Ti–O and Ti–O–N.

The Ti 2p region is between 459.1 eV (anatase TiO_2) and 455.3 eV (N-doped TiO_2). This observation indicates that the central Ti ion is very sensitive to electronic environment of neighboring elements. By introducing more electron rich N into the matrix, the binding energy of Ti can be significantly lowered [49]. The Ti 2p region of anatase TiO_2 and N-doped TiO_2 showed 459.5 and 459.1 eV, respectively.

The binding energy of Ti 2p after nitrogen doping decreases suggests different electronic interactions of Ti with N ion, which causes partial electron transformation from the N to the Ti and an increase of the electron density on Ti because of the lower electro-negativity of nitrogen compared to oxygen [25,29]. This confirms that nitrogen incorporates into the lattice and replaces oxygen. The Ti 2p spectrum for anatase TiO_2 and N-doped TiO_2 are given in Fig. 14. The O 1s XPS spectrum in Fig. 15 also showed significant changes upon nitrogen incorporation. An additional peak for N-doped TiO_2 appears at about 531.7 eV and previously was attributed to the presence of Ti–O–N bonds [48]. The most significant being an additional signal at higher binding energy of 531.7 eV than 530.6 eV was observed. These peak shifts are again possibly due to geometrical constraints in the different nano structures and the additional peak, which appears at 531.7 eV clearly noted in the spectrum of the synthesized N-doped nano TiO_2.

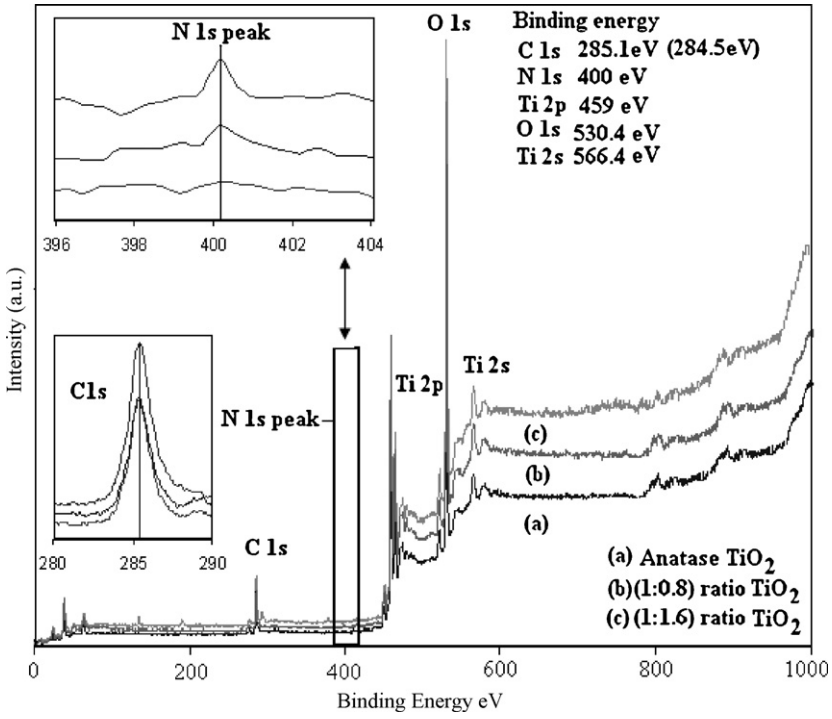

Fig. 13. X-ray photoelectron spectra of pure anatase and N-doped TiO_2 nano-particles.

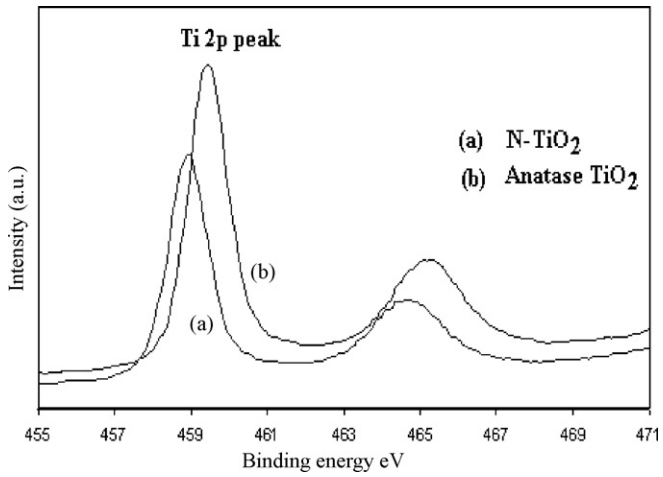

Fig. 14. XPS of Ti 2p spectrum for anatase TiO_2 and N-doped TiO_2 (1:1.6 ratio).

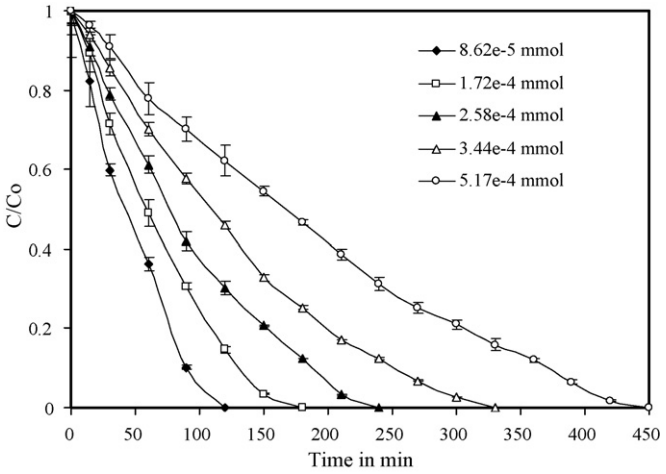

Fig. 16. Kinetics of lindane degradation with varying initial concentrations of lindane by N–TiO_2.

3.5. Effect of lindane concentrations on photocatalytic degradation and degradation pathway

Studies were conducted to evaluate the effect of initial concentrations of lindane on photocatalytic degradation using N-doped TiO_2. Initial concentration of lindane was varied from 8.62×10^{-5} to 5.17×10^{-4} mmol/L. Complete degradation of lindane was achieved for 8.62×10^{-5}, 1.72×10^{-4}, 2.58×10^{-4}, 3.44×10^{-4} and 5.17×10^{-4} mmol/L within 120, 180, 240, 330 and 450 min, respectively. The rate of degradation of lindane gradually decreased with increase in initial pesticide concentration as shown in Fig. 16. A lower photodegradation rate was observed with increasing initial concentration of lindane. This might be due to its high resistance to oxidation via hydroxyl radical attack. Dionysiou et al. [9] have reported that lindane is less prone to oxidation due to its non-aromatic and saturated structure and the absence of a double bond. During the photocatalytic degradation of lindane, only two intermediates namely 1-hydroxy-2,3,4,5,6-pentachlorocyclohexane (m/z 272) and pentachloro cyclohexane (m/z 256) were identified using GC–MS analysis as shown in Fig. 17. The two intermediates appeared in the middle of the reaction and as time progressed, the intermediates gradually disappeared. At the end of the experiment, none of the intermediates were observed in the system. The plausible degradation pathway of lindane is given in Fig. 18. As mentioned earlier, only two intermediates were detected. Other intermediate compounds might have formed and degraded instantaneously. Concentration of free chloride ion, which was formed during the degradation of lindane, was analyzed using ion chromatography (IC). The concentration of free chloride ion was monitored only for two concentration of lindane, i.e. 3.44×10^{-4} (0.10 mg/L) and 5.17×10^{-4} mmol/L (0.15 mg/L). Final free chloride ion concentrations corresponding to these lindane concentrations as per stoichiometry are 0.073 mg/L and 0.1097 mg/L, respectively. The observed concentrations were 0.0523 mg/L and 0.086 mg/L, respectively which accounts for 86% of the total chloride. The slight mismatch may be due to the analytical errors while handling very low concentrations.

3.6. Comparison of lindane degradation under different light sources

The photocatalytic degradation of lindane was carried out with different light sources (UV 365 nm and visible >400 nm) using

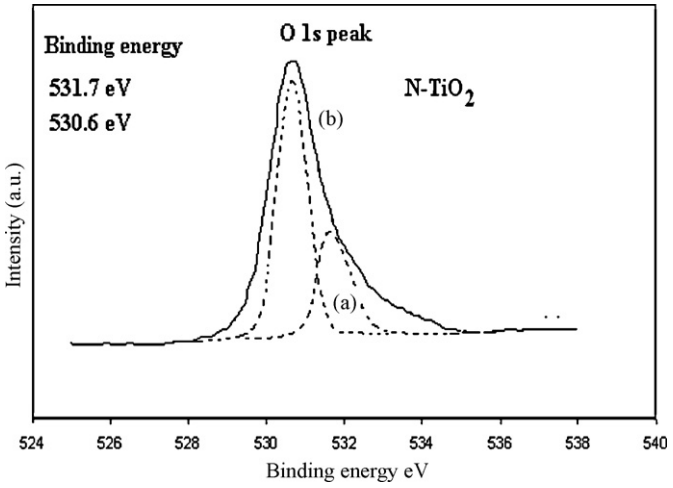

Fig. 15. XPS of O 1s spectrum for anatase TiO_2 and N-doped TiO_2 (1:1.6 ratio).

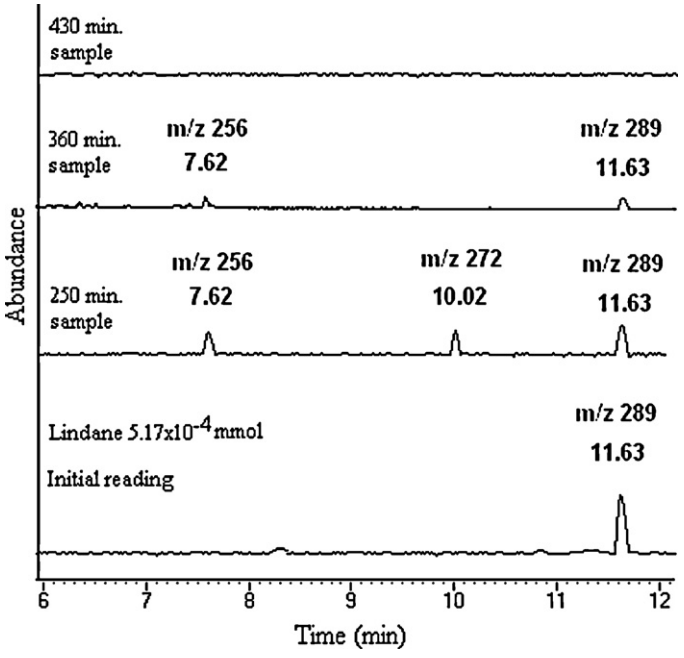

Fig. 17. Identification of intermediates by GC–MS analysis during photodegradation of lindane.

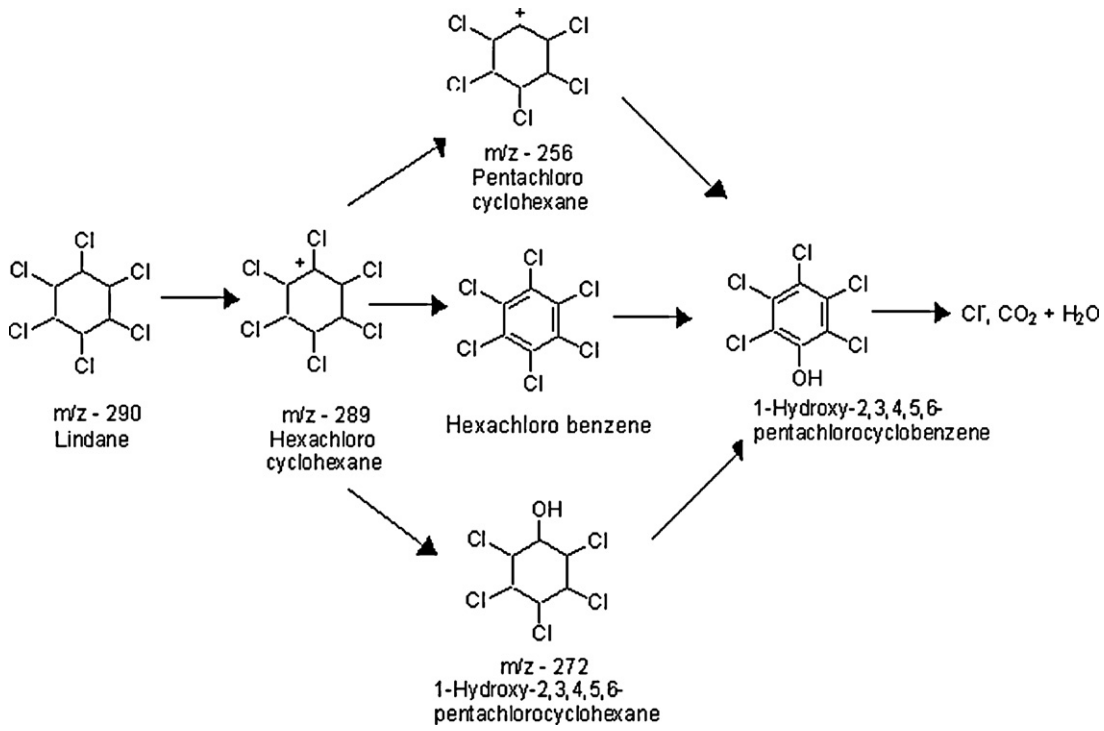

Fig. 18. Proposed pathway of lindane degradation.

Table 2
Degradation of lindane under different light sources.

S. No	Catalysts	Con. (mmol/L)	Kinetics of Lindane					
			UV light			Visible light		
			R^2	k (min^{-1})	% removal	R^2	k (min^{-1})	% removal
1	Degussa P-25	5.17×10^{-4}	0.979	0.099	100	0.693	0.001	13.24
2	Anatase TiO_2	5.17×10^{-4}	0.988	0.117	100	0.777	0.016	20.68
3	N-doped TiO_2	5.17×10^{-4}	0.963	0.007	60	0.909	0.023	100

anatase, Degussa P-25 and N-doped TiO_2. All the other parameters were kept constant. A fixed concentration of 5.17×10^{-4} mmol/L lindane was used for this study. Reaction rates, k (min^{-1}) and R^2 were determined by plots of ln(C/Co) versus time for all the three catalysts and the results are given in Table 2. Degradation of lindane using Degussa P-25 TiO_2 and anatase TiO_2 showed 100% degradation of lindane under UV light, whereas only 13.24% and 20.68% of degradation was observed in the presence of visible light. However in case of N-doped TiO_2, 37.5% and 100% of degradation of lindane was observed under UV and visible light, respectively.

4. Conclusions

N-doped TiO_2 demonstrate photocatalytic activity under visible light irradiation. This was successfully prepared by a modified sol–gel procedure using triethylamine as nitrogen source. Among different nitrogen containing organic compounds triethylamine doped TiO_2 showed better photocatalytic activity compared to other nitrogen containing organic compounds. XRD, SEM and TEM showed that the crystalline size of N-doped TiO_2 was around 22 nm and XPS study confirmed that the N replaces the O in the lattice of TiO_2 in the form of O–Ti–N. The degradation of lindane under visible light using N-doped TiO_2 was found to be satisfactory. GC–MS analysis reveals that the lindane was completely degraded and no intermediate was observed at the end of the analysis.

References

[1] U.K. Sarkar, V.S. Basheer, A.K. Singh, S.M. Srivastava, Organochlorine pesticide residues in water and fish samples: first report from rivers and streams of Kumaon Himalayan region, India, Bull. Environ. Contam. Toxicol. 70 (2003) 485–493.
[2] R.P. Singh, Comparison of organochlorine pesticide levels in soil and ground water of Agra, India, Bull. Environ. Contam. Toxicol. 67 (2001) 126–132.
[3] K. Ramakrishna, L. Philip, Adsorption and desorption characteristics of lindane, carbofuran and methyl parathion on various Indian soils, J. Hazard. Mater. 160 (2008) 559–567.
[4] Y.F. Li, Global technical hexachlorocyclohexane usage and its contamination consequences in the environment: from 1948 to 1997, Sci. Total Environ. 232 (1999) 121–158.
[5] S. Muralidharan, V. Dhananjayan, P. Jayanthi, Organochlorine pesticides in commercial marine fishes of Coimbatore, India and their suitability for human consumption, Environ. Res. 109 (2009) 15–21.
[6] C. Shifu, C. Gengyu, Photocatalytic degradation of organophosphorus pesticides using floating photocatalyst TiO_2:SiO_2/beads by sunlight, Sol. Energy 79 (2005) 1–9.
[7] J.P. Wilcoxon, Photocatalysis using semiconductor nanoclusters, in: MRS Proc., Boston, MA, Adv. Catal. Mater. (1998).
[8] J. Senthilnathan, L. Philip, Removal of mixed pesticides from drinking water system by photodegradation using suspended and immobilized TiO_2, J. Environ. Sci. Health Part B 44 (2009) 262–270.
[9] D.D. Dionysiou, A.P. Khodadoust, A.M. Kern, M.T. Suidan, I. Baudin, J.M. Laine, Continuous-mode photocatalytic degradation of chlorinated phenols and pesticides in water using a bench-scale TiO_2 rotating disk reactor, Appl. Catal. B: Environ. 24 (2000) 139–155.
[10] A. Zaleska, J. Hupkaa, M. Wiergowski, M. Biziuk, Photocatalytic degradation of lindane, p,p o-DDT and methoxychlor in an aqueous environment, J. Photochem. Photobiol. A: Chem. 135 (2000) 213–220.
[11] D.S. Ollis, H. Al-Ekabi, Photocatalytic Purification and Treatment of Water and Air, Elsevier, Amsterdam, 1993.

[12] D. Chatterjee, A. Mahata, Evidence of superoxide radical formation in the photodegradation of pesticide on the dye modified TiO_2 surface using visible light, J. Photochem. Photobiol. A: Chem. 165 (2004) 19–23.
[13] R. Asahi, T. Morikawa, T. Ohwaki, K. Aoki, Y. Taga, Visible-light photocatalysis in nitrogen-doped titanium oxides, Science 293 (2001) 269–271.
[14] Y. Matsumoto, M. Murakami, T. Shono, T. Hasegawa, T. Fukumura, M. Kawasaki, P. Ahmet, T. Chikyow, S. Koshihara, H. Koinuma, Room-temperature ferromagnetism in transparent transition metal-doped titanium dioxide, Science 291 (2001) 854–856.
[15] W. Choi, A. Termin, M.R. Hoffmann, The role of metal ion dopants in quantum-sized TiO_2: correlation between photoreactivity and charge carrier recombination dynamics, J. Phys. Chem. 98 (1994) 13669–13679.
[16] C.D. Valentin, E. Finazzi, G. Pacchioni, A. Selloni, S. Livraghi, M.C. Paganini, E. Giamello, N-doped TiO_2: theory and experiment, Chem. Phys. 339 (2007) 44–56.
[17] X. Yang, C. Cao, L. Erickson, K. Hohn, R. Maghirang, K. Klabunde, Photo-catalytic degradation of rhodamine B on C, S, N, and Fe-doped TiO_2 under visible-light irradiation, App. Catal. B: Environ. 91 (2009) 657–662.
[18] M. Kitano, M. Matsuoka, M. Ueshima, M. Anpo, Recent developments in titanium oxide-based photocatalysts, Appl. Catal. A: Gen. 325 (2007) 1–14.
[19] S. Sato, R. Nakamura, S. Abe, Visible-light sensitization of TiO_2 photocatalysts by wet-method N doping, Appl. Catal. A: Gen. 284 (2005) 131–137.
[20] K. Kobayakawa, Y. Murakami, Y. Sato, Visible-light active N-doped TiO_2 prepared by heating of titanium hydroxide and urea, J. Photochem. Photobiol. A: Chem. 170 (2005) 177–179.
[21] X. Chen, Y. Lou, A.C.S. Samia, C. Burda, J.L. Cole, Formation of oxinitride as the photocatalytic enhancing site in nitrogen doped titania nanocatalysts: compare to a commercial nano powder, Adv. Funct. Mater. 15 (2005) 41–49.
[22] T. Ohno, M. Akiyoshi, T. Umebayashi, K. Asai, T. Mitsui, M. Matsumura, Preparation of S-doped TiO_2 photocatalysts and their photocatalytic activities under visible light, Appl. Catal. A: Gen. 265 (2004) 115–121.
[23] J. Ananpattarachai, P. Kajitvichyanukul, S. Seraphin, Visible light absorption ability and photocatalytic oxidation activity of various interstitial N-doped TiO_2 prepared from different nitrogen dopants, J. Hazard. Mater. 168 (2009) 253–261.
[24] M. Xing, J. Zhang, F. Chen, New approaches to prepare nitrogen-doped TiO_2 photocatalysts and study on their photocatalytic activities in visible light, Appl. Catal. B: Environ. 89 (2009) 563–569.
[25] Y. Cong, J. Zhang, F. Chen, M. Anpo, Synthesis and characterization of nitrogen-doped TiO_2 nanophotocatalyst with high visible light activity, J. Phys. Chem. C 111 (2007) 6976–6982.
[26] Y. Huan, Z. Xuxu, Y. Zhongyi, T. Feng, F. Beibei, H. Keshan, Preparation of nitrogen-doped TiO_2 nanoparticle catalyst and its catalytic activity under visible light, Chin. J. Chem. Eng. 15 (2007) 802–807.
[27] R. Kun, S. Tarjan, A. Oszko, T. Seemann, V. Zollmer, M. Busse, I. Dekany, Preparation and characterization of mesoporous N-doped and sulfuric acid treated anatase TiO_2 catalysts and their photocatalytic activity under UV and Vis illumination, J. Solid State Chem. 182 (2009) 3076–3084.
[28] K.A. Michalow, D. Logvinovich, A. Weidenkaff, M. Amberg, G. Fortunato, A. Heel, T. Graule, M. Rekas, Synthesis, characterization and electronic structure of nitrogen-doped TiO_2 nanopowder, Catal. Today 144 (2009) 7–12.
[29] M. Sathish, B. Viswanathan, R.P. Viswanath, Characterization and photocatalytic activity of N-doped TiO_2 prepared by thermal decomposition of Ti–melamine complex, Appl. Catal. B: Environ. 74 (2007) 307–312.
[30] Z. Wu, F. Dong, W. Zhao, S. Guo, Visible light induced electron transfer process over nitrogen doped TiO_2 nanocrystals prepared by oxidation of titanium nitride, J. Hazard. Mater. 157 (2008) 57–63.
[31] S. Chen, P. Zhang, D. Zhuang, W. Zhu, Investigation of nitrogen doped TiO_2 photocatalytic films prepared by reactive magnetron sputtering, Catal. Commun. 5 (2004) 677–680.
[32] W. Zuyuan, Z. Fuxiang, Y. Yali, C. Jie, S. Qing, G. Naijia, One-pot synthesis of visible-light-responsive TiO_2 in the presence of various amines, Chin. J. Catal. 27 (2006) 1091–1095.
[33] J. Yu, J. Wang, J. Zhang, Z. He, Z. Liu, X. Ai, Characterization and photoactivity of TiO_2 sols prepared with triethylamine, Mater. Lett. 61 (2007) 4984–4988.
[34] C. Burda, Y. Lou, X. Chen, A.C.S. Samia, J. Stout, J.M. Gole, Enhanced nitrogen doping in TiO_2 nanoparticles, Nano Lett. 3 (2003) 1049–1051.
[35] H. Tokudome, M. Miyauchi, N-doped TiO_2 nanotube with visible light activity, Chem. Lett. 33 (2004) 1108–1109.
[36] B. O'Regan, M. Gratzel, A low-cost, high-efficiency solar cell based on dye-sensitized colloidal TiOz films, Nature 353 (1991) 737–740.
[37] Y. Choi, T. Umebayashi, M. Yoshikawa, Fabrication and characterization of C-doped anatase TiO_2 photocatalysts, J. Mater. Sci. 39 (2004) 1837–1839.
[38] G. Li, L. Chen, N.M. Dimitrijevic, K.A. Gray, Visible light photocatalytic properties of anion-doped TiO_2 materials prepared from a molecular titanium precursor, Chem. Phy. Lett. 451 (2008) 75–79.
[39] J. Pielaszek, X-ray diffraction from nanostructured materials, in: K. Philippe, S. Joop (Eds.), Nanostructured Materials: Selected Synthesis Methods, Properties and Applications, Kluwer Academic Publishers, Boston, 2002, pp. 127–143.
[40] S.U.M. Khan, M. Al-Shahry, W.B. Ingler, Efficient photochemical water splitting by a chemically modified n-TiO_2, Science 297 (2002) 2243–2245.
[41] T.D. Robert, L.D. Laude, V.M. Geskin, R. Lazzaroni, R. Gouttebaron, Micro-Raman spectroscopy study of surface transformations induced by excimer laser irradiation of TiO_2, Thin Solid Films 440 (2003) 268–277.
[42] H. Tang, K. Prasad, R. Sanjinbs, P.E. Schmid, F. Levy, Electrical and optical properties of TiO_2 anatase thin films, J. Appl. Phys. 75 (1994) 2042–2047.
[43] D. Bersani, G. Antonioli, P.P. Lottici, T. Lopez, Raman study of nanosized titania prepared by sol–gel route, J. Non-Cryst. Solids 232–234 (1998) 175–181.
[44] M. Bernard, A. Deneuville, O. Thomas, P. Gergaud, P. Sandstrom, J. Birch, Raman spectra of TiN/AlN super lattices, Thin Solid Films 380 (2000) 252–255.
[45] Y.H. Cheng, B.K. Tay, S.P. Lau, H. Kupfer, F. Richter, Substrate bias dependence of Raman spectra for TiN films deposited by filtered cathodic vacuum arc, J. Appl. Phys. 92 (2002) 1845–1849.
[46] R. Nakamura, T. Tanaka, Y. Nakato, Mechanism for visible light responses in anodic photocurrents at N-doped TiO_2 film electrodes, J. Phys. Chem. B 108 (2004) 10617–10620.
[47] O. Diwald, T.L. Thompson, T.E. Zubkov, G. Goralski, S.D. Walck, J.T. Yates, Photochemical activity of nitrogen-doped rutile TiO_2(1 1 1) in visible light, J. Phys. Chem. B 108 (2004) 6004–6008.
[48] N.C. Saha, H.C. Tomkins, Titanium nitride oxidation chemistry: an X-ray photoelectron spectroscopy study, J. Appl. Phys. 72 (1992) 3072–3079.
[49] X. Chen, C. Burda, Photoelectron spectroscopic investigation of nitrogen-doped. Titania nanoparticles, J. Phys. Chem. B 108 (2004) 15446–15449.